JJEE

Volume 12 | Number 2 | June 2026 | Pages 225-247

Jordan Journal of Electrical Engineering

ISSN (print): 2409-9600, ISSN (online): 2409-9619

Homepage: jjee.ttu.edu.jo

Optimizing Virtual Synchronous Generator Behavior in MMCs via Super Twisting Algorithm for Improved Grid Stability

M. Chethan[1], Dr. Ravi.k[2*]

[1, 2] School of Electrical Engineering, Vellore Institute of Technology, Vellore, Tamil Nadu -632014, India
E-mail: k.ravi@vit.ac.in

Received: Aug 25, 2025 *Revised: Jan 12, 2026* *Accepted: Jan 30, 2026* *Available online: Jun 15, 2026*

***Abstract*—** Ensuring stable grid synchronization in Modular Multilevel Converters that replicate the behaviour of Virtual Synchronous Generators is essential for maintaining reliable power system performance and achieving optimal dynamic response. This paper proposes a novel optimization strategy for VSG control within MMCs, utilizing a super-twisting algorithm-based sliding mode to systematically adjust key parameters such as synthetic inertia, damping coefficients, and power-frequency droop settings. Through continuous adaptation of these control parameters, the system enhances its ability to regulate frequency and voltage with greater accuracy, particularly under mild disturbances and variable grid conditions. The proposed method improves the converter's responsiveness and stability, enabling it to better emulate synchronous machine characteristics in real-time. Extensive simulation studies conducted across diverse operating scenarios highlight the effectiveness of the approach. Notable improvements include faster synchronization with grid frequency, accelerated stabilization following disturbances, improved voltage recovery, and stronger attenuation of oscillations. The algorithm's ability to fine-tune control dynamics in response to changing conditions contributes to a more resilient and adaptive power conversion system. Moreover, the framework demonstrates high flexibility and robustness, making it well-suited for integration into future smart grid environments characterized by inverter-based generation and distributed energy resources. By enhancing the dynamic behaviour and control precision of VSG-enabled MMCs, this technique offers a compelling solution for modern power systems that demand both reliability and adaptability. The STA-SM control framework delivers marked enhancements compared to the conventional VSG approach. Numerical evaluation indicates a substantial decrease in total harmonic distortion (THD) by 42.9%, alongside a 75% improvement in settling time and a 66.7% reduction in frequency deviation, all of which contribute to stronger dynamic stability. Reactive power output is lowered by 83.75%, demonstrating superior regulation capability.

***Keywords*—** Modular multilevel converters (MMCs); Virtual synchronous generators (VSG); Sliding mode controller based super twisting algorithm; Active and reactive power control.

1. INTRODUCTION

The Modular Multilevel Converter has emerged as the preferred voltage source converter in contemporary industrial applications, particularly in scenarios demanding high-voltage and high-power performance. The MMC offers several distinct advantages over conventional multilevel converter topologies [1]. Its architecture, based on a series arrangement of submodules, enables scalable multilevel output, thereby minimizing harmonic distortion and enhancing waveform quality. This configuration not only improves the converter's adaptability and efficiency in power distribution but also facilitates effective handling of lower voltage levels, making it suitable for a diverse range of power conversion environments.

* Corresponding author

DOI: https://doi.org/ 10.5455/jjee.204-1756367315

In grid-connected inverter systems, the MMC contributes to improved output waveform fidelity while simultaneously advancing the overall efficiency, reliability, and cost-effectiveness of the converter infrastructure. Its versatility supports a broad spectrum of applications across industrial and utility domains [2]. Typically, MMC-based grid integration relies on control strategies such as vector control and droop control. Vector control ensures precise tracking of reference active and reactive power values; however, it lacks the adaptability required to respond dynamically to variations in the AC grid, limiting its effectiveness under adverse grid conditions [3]. Conversely, droop control facilitates decentralized voltage and frequency regulation but encounters limitations when subjected to abrupt frequency shifts or grid disturbances.

Although conventional control strategies offer certain advantages, Modular Multilevel Converter systems operating under traditional grid-connected frameworks continue to encounter limitations. These include inefficient grid synchronization, insufficient inertial emulation, restricted grid support functionality, inadequate damping of oscillatory modes, and delayed dynamic response. To better understand inverter behavior in grid-connected scenarios, comparative analyses with synchronous generators have been conducted. In such studies, inertia and damping parameters are typically derived from the system's rated power and synchronous angular velocity. However, the intrinsic link between these parameters and the inverter's internal architecture remains ambiguous.

Existing literature suggests that the mathematical formulations and physical principles governing pulse-width modulated (PWM) grid-tied inverters share notable similarities with those of rotating synchronous machines [4]. To emulate the inertial and damping characteristics of synchronous generators, static models incorporating DC capacitors and voltage sources have been employed. Various enhancements to Virtual Synchronous Generator control have been proposed, including the refinement of V_{2-P} droop characteristics and tuning of control parameters to improve damping behaviour. Grid-forming control has also been integrated with VSG frameworks to develop inverters capable of providing grid support functionalities, as depicted in (Fig.1). Within MMC systems, VSG-based control schemes utilize DC voltage and equivalent capacitance to define the primary controller's inertia parameters [5].

Recent advancements include the application of deep reinforcement learning techniques, such as the TD3-based adaptive controller, to optimize VSG performance in MMC configurations [6]. These adaptive modules have demonstrated improved system stability and dynamic response in simulation environments [7]. To address frequency stability challenges in Voltage Source Converter–High Voltage Direct Current systems, adaptive neuro-fuzzy control strategies have been introduced. These approaches dynamically adjust virtual inertia and damping coefficients to enhance oscillation suppression across varying operational conditions [8].

Further innovations involve the incorporation of a first-order low-pass filter within the voltage feed-forward path to reduce the MMC's resonant frequency, alongside a second-order filterfunctionally similar to a notch filter within the current feedback loop to precisely shape impedance characteristics and mitigate both sub-synchronous and high-frequency oscillations [9]. To elevate VSG performance, researchers have proposed an adaptive optimization framework utilizing fuzzy logic controllers for real-time adjustment of inertia and damping parameters. The differential evolution algorithm is employed to fine-tune FLC gains, resulting

in enhanced frequency stability under grid disturbances and fluctuating levels of renewable energy integration [10]. For MMC-HVDC systems, a range of control methodologies including droop control, rate-of-change-of-frequency (df/dt) control, virtual inertia emulation, and VSG-based strategies have been explored to address the frequency stability issues arising from reduced system inertia [11].

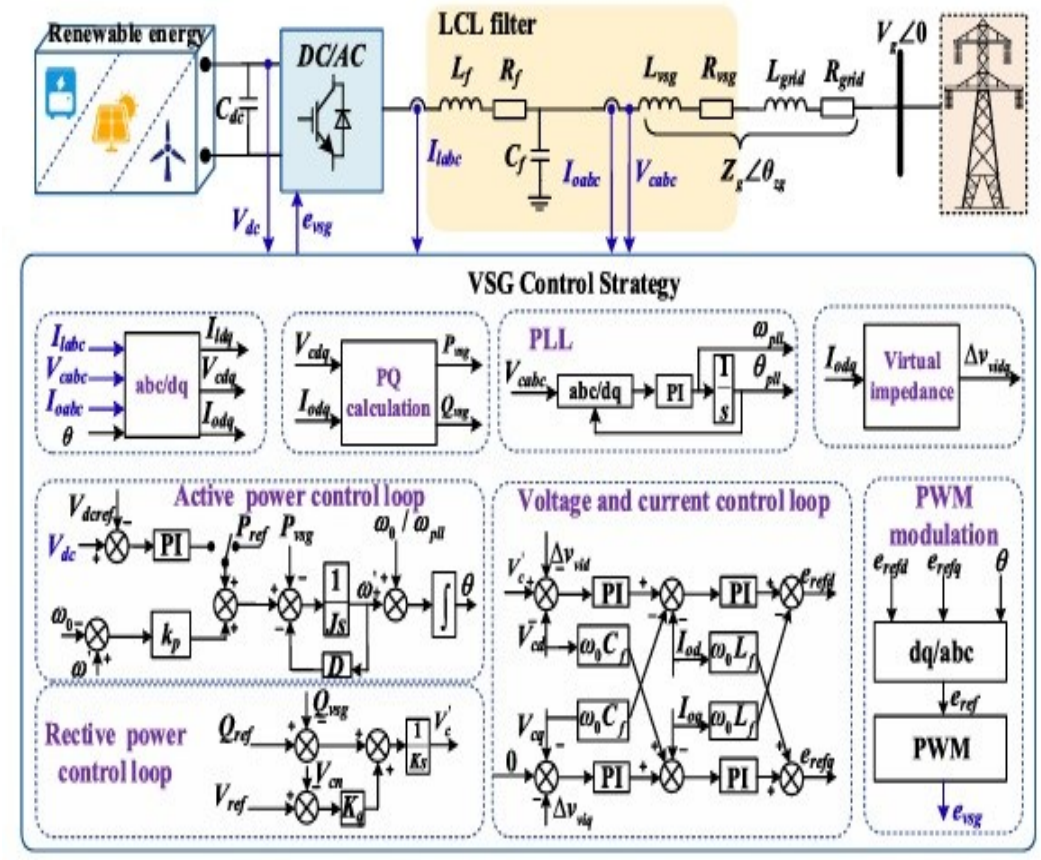

Fig. 1. Inverter-based VSG algorithm.

Virtual Synchronous Generator control has emerged as a compelling strategy for emulating the dynamic characteristics of conventional synchronous machines, thereby introducing synthetic inertia and damping into converter-based systems [12]. This capability is particularly valuable in enhancing the stability and transient response of power systems with substantial integration of renewable energy sources and Voltage Source Converter–based High Voltage Direct Current links. Accordingly, this study is driven by the imperative to refine VSG control mechanisms for MMC-based VSC-HVDC systems, with the objective of mitigating power system oscillations effectively.

Despite notable progress in the field, optimizing VSG control within MMC-based VSC-HVDC architectures presents several technical challenges. Chief among these is the complex and context-sensitive process of parameter tuning, which is influenced by operating conditions and grid-specific attributes [13]. The proposed impedance shaping methodology incorporates a first-order low-pass filter in the voltage feed-forward path and a second-order filter in the current feedback loop to achieve targeted frequency response characteristics [14]. Integrating these filtering elements while maintaining control system stability and performance demands careful engineering consideration. Moreover, the deployment of

advanced VSG algorithms is often computationally intensive and constrained by hardware limitations, including processor speed, memory capacity, and communication latency.

To address fault conditions, recent work has introduced an enhanced VSG fault control strategy that supports voltage regulation and sustains synthetic inertia and damping during unbalanced grid events [15]. This approach utilizes a high-pass filter within the damping loop to eliminate active power deviations and dynamically adjust damping coefficients, thereby improving droop control behaviour and overall system damping [16].

In addition, small-signal modelling techniques have been employed to investigate the dynamic interactions between MMCs and synchronous generators. Eigenvalue analysis reveals that under low-inertia conditions, the control coupling between these components significantly influences low-frequency oscillatory modes [17]. Ensuring the robustness of VSG control against a range of disturbances, including grid faults, cyber intrusions, and submodule malfunctions, is essential for dependable system operation. Scaling VSG strategies to multi-terminal HVDC networks comprising multiple MMC units introduces further complexity. Centralized control schemes may suffer from scalability issues and vulnerability to single-point failures. In contrast, decentralized architecture offers improved resilience but require sophisticated coordination and data exchange mechanisms among distributed controllers to maintain system-wide stability [18].

The advancements in Virtual Synchronous Generator control, with a particular focus on mitigating low-frequency oscillations in power systems. The study introduces a supplementary damping controller aimed at enhancing active oscillation suppression without compromising the steady-state power output of the VSG as shown in (Fig.1). Through an analytical investigation of the interaction between the VSG and a Single Machine Infinite Bus model, the proposed controller is shown to be effective in improving dynamic stability an essential consideration for optimizing control in MMC-based VSC-HVDC systems [19].

Despite these innovations, the practical deployment of VSG control faces several challenges. Factors such as sensor noise, latency in communication channels, and hardware constraints can adversely affect control accuracy and system resilience [20]. Addressing these issues necessitates ongoing research into more robust control algorithms, efficient hardware-software integration, and comprehensive real-time validation. Overcoming these barriers is critical to developing high-performance VSG strategies for MMC-based VSC-HVDC systems, thereby enabling reliable integration of renewable energy sources into future grid infrastructures [21].

This research aims to bridge existing gaps in VSG control methodologies tailored for MMC–VSC–HVDC applications [22]. Conventional VSG implementations often suffer from insufficient synthetic inertia, which can compromise frequency stability, particularly in grids with high renewable penetration. Additionally, many existing approaches lack adequate damping capabilities, resulting in prolonged oscillatory behaviour and reduced system reliability [23].

Another pressing concern is the diminished effectiveness of current VSG control schemes under weak grid conditions. Such environments can lead to instability in voltage and frequency, undermining overall system robustness [24]. Moreover, the slow responsiveness of certain VSG algorithms to transient disturbances such as abrupt load variations or fault events further limits their practical utility. The inherent complexity of these control frameworks also poses challenges for real-time deployment and parameter tuning [25]. To address these

limitations, this study proposes enhancements to VSG control strategies specifically designed for VSC-HVDC systems to improve dynamic performance, fault tolerance, and grid compatibility [26].

The proposed simulation framework has been explicitly verified against benchmark MMC/VSG models documented in recent literature [27,28]. Comparative results confirm consistency in transient stability, frequency regulation, and capacitor voltage balancing.

2. CHARACTERIZATION AND MODELLING OF GRID-TIED MMC SYSTEMS

The Modular Multilevel Converter (MMC) has emerged as a preferred topology for high-power grid integration due to its scalability, modularity, and superior harmonic performance [29]. In a grid-tied configuration, the MMC acts as the interface between a DC source and the AC grid, enabling bidirectional power exchange and stable operation under varying grid conditions [30].

(a) Main Circuit

Fig.2 depicts the equivalent circuit of the MMC. In Fig.2, u_{dcu} and u_{dcl} represent DC voltages of the positive and negative poles, respectively, each with a value of $1/2u_{dc}$; i_{dc} is the DC side current; i_{uA}, $i_{lA,}$ and u_{cumA}, u_{clmA} denote the upper and lower arm currents and voltages, respectively; i_{cA} represents the circulating current; u_{mA} and $i_{mA,}$ respectively, refer to the phase A voltage and current on the AC side; R_{arm} and L_{arm} are the equivalent arm impedances.

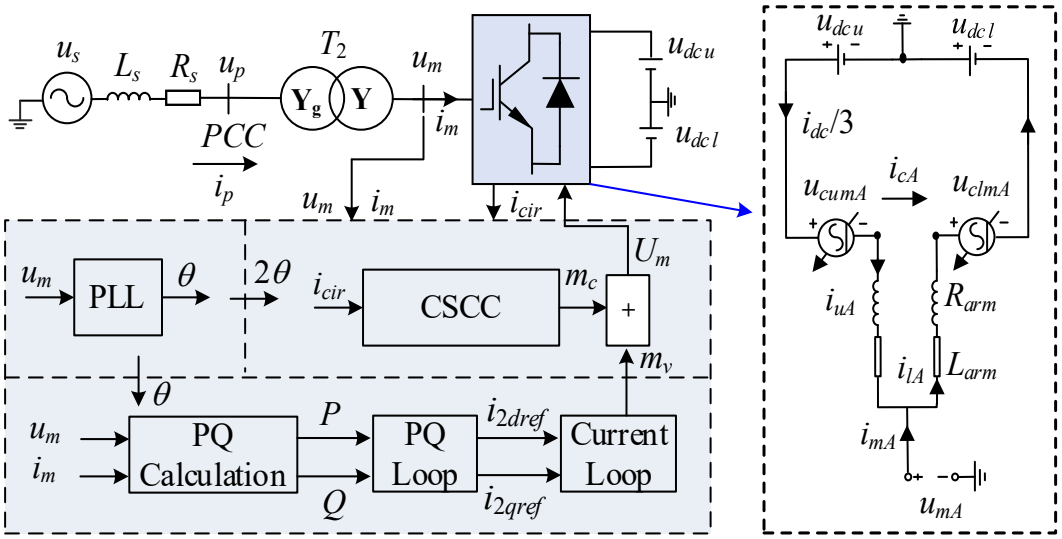

Fig. 2. Equivalent circuit of a single-phase MMC.

Applying the KVL to the circuit, the equations of phase A can be obtained as (Eq.1):

$$\begin{cases} \dfrac{di_{cA}}{dt} = -\dfrac{R_{arm}}{L_{arm}} i_{cA} - \dfrac{n_{uA}}{2L_{arm}} u_{cumA} - \dfrac{n_{lA}}{2L_{arm}} u_{clmA} + \dfrac{u_{dc}}{2L_{arm}} \\ \dfrac{di_{mA}}{dt} = -\dfrac{R_{arm}}{L_{arm}} i_{mA} + \dfrac{n_{uA}}{L_{arm}} u_{cumA} - \dfrac{n_{lA}}{L_{arm}} u_{clmA} + \dfrac{2u_{mA}}{L_{arm}} \\ \dfrac{du_{cumA}}{dt} = \dfrac{N_m n_{uA}}{C} i_{cA} - \dfrac{N_m n_{uA}}{2C} i_{mA} \\ \dfrac{du_{clmA}}{dt} = \dfrac{N_m n_{lA}}{C} i_{cA} + \dfrac{N_m n_{lA}}{2C} i_{2A} \end{cases} \quad (1)$$

where n_{uA} and n_{lA} represent the modulation signals for the upper and lower arm of Phase A; N_m is the number of Submodules.

Based on HSS, the three-phase main circuit of the MMC can be formulated in HSS

domain, as:

$$\begin{cases} \dfrac{d\boldsymbol{i}_{cj}}{dt} = [-\dfrac{R_{arm}}{L_{arm}}\boldsymbol{EI} - \boldsymbol{N}]\boldsymbol{i}_{cj} - \dfrac{\Gamma(n_{uj})}{2L_{arm}}\boldsymbol{u}_{cumj} - \dfrac{\Gamma(n_{lj})}{2L_{arm}}\boldsymbol{u}_{clmj} + \dfrac{\boldsymbol{u}_{dc}}{2L_{arm}} \\ \dfrac{d\boldsymbol{i}_{mj}}{dt} = [-\dfrac{R_{arm}}{L_{arm}}\boldsymbol{EI} - \boldsymbol{N}]\boldsymbol{i}_{mj} + \dfrac{\Gamma(n_{uj})}{L_{arm}}\boldsymbol{u}_{cumj} - \dfrac{\Gamma(n_{lj})}{L_{arm}}\boldsymbol{u}_{clmj} + \dfrac{2\boldsymbol{u}_{mj}}{L_{arm}} \\ \dfrac{d\boldsymbol{u}_{cumj}}{dt} = [0 \times \boldsymbol{EI} - \boldsymbol{N}]\boldsymbol{u}_{cumj} + \dfrac{N_m\Gamma(n_{uj})}{C}\boldsymbol{i}_{cj} - \dfrac{N_m\Gamma(n_{uA})}{2C}\boldsymbol{i}_{mj} \\ \dfrac{d\boldsymbol{u}_{clmj}}{dt} = [0 \times \boldsymbol{EI} - \boldsymbol{N}]\boldsymbol{u}_{clmj} + \dfrac{N_m\Gamma(n_{lj})}{C}\boldsymbol{i}_{cj} + \dfrac{N_m\Gamma(n_{lj})}{2C}\boldsymbol{i}_{mj} \end{cases} \quad (2)$$

(b) PQ control loop

According to the control diagram in Fig. 2, the MMC converter employs a PQ control loop, which includes an outer PQ control and an inner current control. In the HSS domain, the park transformation can be expressed as:

$$\begin{cases} \boldsymbol{u}_{md} = \Gamma[\cos(\omega_0 t)] \times \boldsymbol{u}_{mA} + \Gamma[\cos(\omega_0 t - \dfrac{2\pi}{3})] \times \boldsymbol{u}_{mB} + \Gamma[\cos(\omega_0 t + \dfrac{2\pi}{3})] \times \boldsymbol{u}_{mC} \\ \boldsymbol{u}_{mq} = -\Gamma[\sin(\omega_0 t)] \times \boldsymbol{u}_{mA} - \Gamma[\sin(\omega_0 t - \dfrac{2\pi}{3})] \times \boldsymbol{u}_{mB} - \Gamma[\sin(\omega_0 t + \dfrac{2\pi}{3})] \times \boldsymbol{u}_{mC} \\ \boldsymbol{i}_{2d} = \Gamma[\cos(\omega_0 t)] \times \boldsymbol{i}_{mA} + \Gamma[\cos(\omega_0 t - \dfrac{2\pi}{3})] \times \boldsymbol{i}_{mB} + \Gamma[\cos(\omega_0 t + \dfrac{2\pi}{3})] \times \boldsymbol{i}_{mC} \\ \boldsymbol{i}_{2q} = -\Gamma[\sin(\omega_0 t)] \times \boldsymbol{i}_{mA} - \Gamma[\sin(\omega_0 t - \dfrac{2\pi}{3})] \times \boldsymbol{i}_{mB} - \Gamma[\sin(\omega_0 t + \dfrac{2\pi}{3})] \times \boldsymbol{i}_{mC} \end{cases} \quad (3)$$

where u_{md}, u_{mq} and i_{md}, i_{mq} are the dq-axis components of u_{mABC} and i_{mABC}. In subsequent analysis, the subscript dq represents the dq-axis component. Then the outer AC voltage control can be derived as:

$$\begin{cases} \boldsymbol{i}_{mdref} = k_{mmcp}(\boldsymbol{P} - \boldsymbol{P}_{ref}) + k_{mmci}\boldsymbol{x}_{P2d} \\ \boldsymbol{i}_{mqref} = k_{mmcp}(\boldsymbol{Q} - \boldsymbol{Q}_{ref}) + k_{mmci}\boldsymbol{x}_{Q2q} \\ \dfrac{d\boldsymbol{x}_{P2d}}{dt} = [-\boldsymbol{N}] \times \boldsymbol{x}_{ugd} + (\boldsymbol{P} - \boldsymbol{P}_{ref}) \\ \dfrac{d\boldsymbol{x}_{Q2q}}{dt} = [-\boldsymbol{N}] \times \boldsymbol{x}_{ugq} + (\boldsymbol{Q} - \boldsymbol{Q}_{ref}) \end{cases} \quad (4)$$

In (Eq.4), x_{P2d} and x_{Q2q} are the integral state variables; P_{ref} and Q_{ref} are the PQ control loop references; k_{mmcp} and k_{mmci} are proportional and integral parameters of the PI controller in the PQ control.

Based on Fig. 2, the inner current control can be written as:

$$\begin{cases} \boldsymbol{U}_{MMCd} = \boldsymbol{u}_{md} - \omega L_{arm}\boldsymbol{i}_{mq} - k_p(\boldsymbol{i}_{mdref} - \boldsymbol{i}_{md}) - k_i\boldsymbol{x}_{imd} \\ \boldsymbol{U}_{MMCq} = \boldsymbol{u}_{mq} + \omega L_{arm}\boldsymbol{i}_{md} - k_p(\boldsymbol{i}_{mqref} - \boldsymbol{i}_{mq}) - k_i\boldsymbol{x}_{imq} \\ \dfrac{d\boldsymbol{x}_{imd}}{dt} = [-\boldsymbol{N}] \times \boldsymbol{x}_{imd} + (\boldsymbol{i}_{mdref} - \boldsymbol{i}_{md}) \\ \dfrac{d\boldsymbol{x}_{imq}}{dt} = [-\boldsymbol{N}] \times \boldsymbol{x}_{imq} + (\boldsymbol{i}_{mqref} - \boldsymbol{i}_{mq}) \end{cases} \quad (5)$$

where x_{im} is the integral state variable of the current control; U_{MMC} is the 50Hz modulation signal; k_p and k_i are proportional and integral parameters of the PI controller used in the current control.

(c) CCSC control

The second harmonic circulating current is suppressed by the CCSC in Fig. 2 and the corresponding HSS model is:

$$\begin{cases} \boldsymbol{U}_{cird} = -2\omega L_{arm}\boldsymbol{i}_{cirq} - k_{cirp}(0\times \boldsymbol{EI} - \boldsymbol{i}_{cird}) - k_{ciri}\boldsymbol{x}_{cird} \\ \boldsymbol{U}_{cirq} = 2\omega L_{arm}\boldsymbol{i}_{cird} - k_{cirp}(0\times \boldsymbol{EI} - \boldsymbol{i}_{cirq}) - k_{ciri}\boldsymbol{x}_{cirq} \\ \dfrac{\boldsymbol{x}_{cird}}{dt} = [-N]^{*}\boldsymbol{x}_{cird} + (0\times \boldsymbol{EI} - \boldsymbol{i}_{cird}) \\ \dfrac{\boldsymbol{x}_{cirq}}{dt} = [-N]^{*}\boldsymbol{x}_{cirq} + (0\times \boldsymbol{EI} - \boldsymbol{i}_{cirq}) \end{cases} \quad (6)$$

where x_{cir} is the integral state variable in the CCSC control; i_{cir} is the circulating current; U_{cir} is the 100Hz modulation signal; k_{cirp} and k_{ciri} are proportional and integral parameters of the PI controller in the CCSC control.

(d) PLL

PLL is a key control module in achieving stable power transmission. Its HSS model is as follows:

$$\begin{cases} \boldsymbol{\omega} = \boldsymbol{\omega}_0 + k_{pllp} * \boldsymbol{u}_{1q} + k_{plli} * \boldsymbol{x}_{pll} \\ \dfrac{d\boldsymbol{x}_{pll}}{dt} = -\boldsymbol{N} * \boldsymbol{x}_{pll} + \boldsymbol{u}_{mq} \\ \dfrac{d\boldsymbol{\theta}}{dt} = -\boldsymbol{N} * \Delta\boldsymbol{\theta} + \boldsymbol{\omega} \end{cases} \quad (7)$$

In Eq. (7), ω_0= 2π*50; x_{pll} is the integral state variable of the PLL; k_{pllp} and k_{plli} are proportional and integral parameters of the PLL.

The schematic illustrates a comprehensive control architecture for a grid-connected power converter interfaced through a transformer and line impedance. The AC source, characterized by voltage u_k, inductance Lx, and resistance Rx, connects to the Point of Common Coupling, where synchronization and power exchange occur. The converter receives input voltage um and current im, and regulates its DC link voltages U_{dc1}, $U_{dc2,}$ and current i_{dc} through coordinated control loops. A Phase-Locked Loop (PLL) extracts the grid angle θ from U_m, enabling transformation of measured quantities into the dq reference frame. The active and reactive power components P and Q are computed and processed through a PQ control loop to generate reference currents i_{dqref}. These are tracked by the current control loop, which outputs i_{dq} to the Current Synchronous Control Component (CSCC). The CSCC generates modulation signals mα, mβ, which are used to synthesize the control voltage Um. The entire system ensures accurate power regulation, grid synchronization, and dynamic response under varying grid conditions.

3. VSG CONTROL OF HYBRID TOPOLOGY MMC

The parameters managed by a VSG in an MMC system are all virtual quantities that do not correspond directly to the physical values of a VSG. The current power system is quite complex in terms of mechanical and electrical power [31]. For clarity, the mechanical power Pm can be linked to the MMC DC power inverter, while the electrical power Pe pertains to the power linked with the grid. Despite this simplification, technologies that employ virtual synchronous generators continue to function effectively. An improved 2nd-order equation is used to describe the mechanical and electrical transient process of the synchronous generator, enabling more efficient analysis of the generator's motion equations [32].

The complete control system of the MMC, derived from the VSG, includes active and reactive power controllers, along with an internal voltage and current controller, as illustrated

in (Fig.3). Unlike traditional double closed-loop vector control, the MMC converter station operating under VSG control can actively influence the frequency and voltage of the AC grid [33]. This helps maintain stable voltage amplitude and frequency on the AC side. VSG control also allows for effective monitoring and adjustment of both active and reactive power. It also incorporates droop control to address any power imbalances within the system, significantly enhancing operational reliability [34]. By carefully adjusting the inertia constant J and damping factor Dp in the VSG, the system's frequency support and oscillation damping capabilities can be improved, thus increasing its robustness [35].

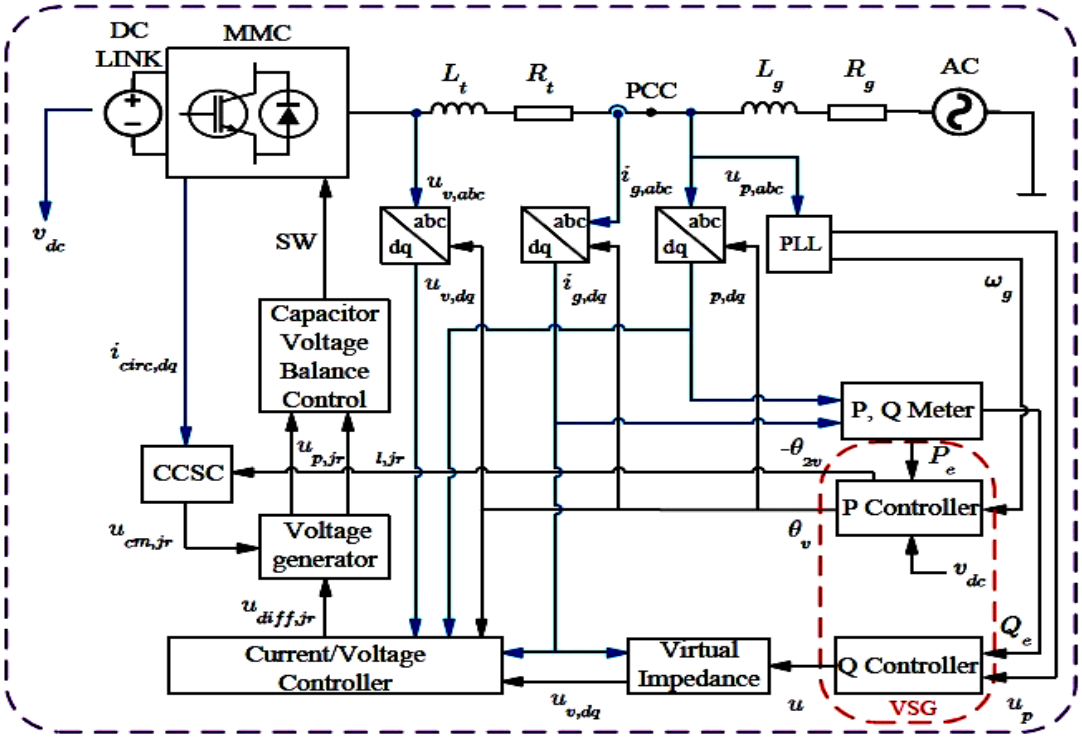

Fig. 3. Grid-tied VSG-based MMC.

4. SUPER-TWISTING ALGORITHM METHODS

Incorporating the Super twisting algorithm framework introduces a highly effective method for addressing synchronization issues prevalent in Modular Multilevel Converter systems operating under Virtual Synchronous Generator control. This nonlinear control enhancement enables the system to better withstand grid variability and model uncertainty conditions frequently observed in renewable energy environments. Unlike conventional synchronization approaches such as phase-locked loops or linear regulators, which tend to respond slowly and suffer from steady-state errors during disturbances, the STA solution delivers rapid alignment of frequency and phase, thus maintaining consistent grid-following performance even amid severe fluctuations.

The dual-loop configuration featuring an external VSG-based power control layer and an internal current-regulation loop facilitates independent modulation of active and reactive components. Integrated observer and feedforward mechanisms further accelerate dynamic estimation and enhance real-time adaptability. One of the most compelling advantages of STA is its inherent suppression of chattering, which results in cleaner switching actions and improved current waveforms, ultimately boosting power quality and extending the durability of converter hardware [36]. Additionally, the control design's synergy with modern pulse-

width modulation schemes allows for fine-tuned current injection and tight synchronization with grid voltage profiles. To ensure precise power decoupling in Virtual Synchronous Generator control within a grid-connected system, the Sliding-Mode Control technique is employed due to its notable advantages in delivering rapid dynamic response and exhibiting strong resilience against parameter uncertainties and external disturbances. The initial stage in STA design involves establishing the baseline model, which serves as a critical foundation for defining the targeted performance characteristics of the system. These combined features demonstrate the STA approach's strong potential for advanced grid interfacing, especially in scenarios demanding scalable control, fast transient response, and robust disturbance rejection, as shown in (Fig. 4).

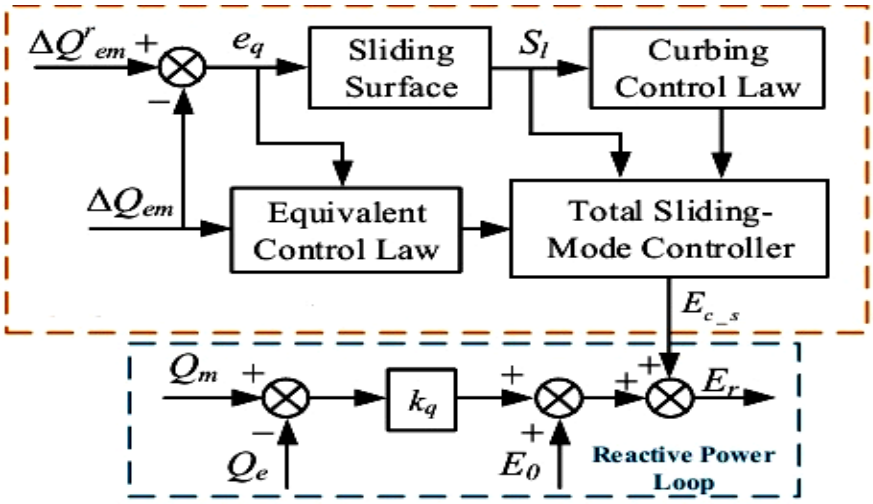

Fig. 4. Control diagram Vsg-based STA control.

Traditional STAs' rapid switching between control states causes this undesirable high-frequency oscillation. STA offers a smoother control approach, minimising or eliminating these oscillations by using continuous, rather than discontinuous, control actions [37]. This results in smoother transitions and less switching overall, achieved through a more gradual switching mechanism. Incorporating both the sliding variable and its first and second derivatives, as shown in (Fig. 5). This allows for more precise tracking of the target while maintaining smooth control output. The STA approach serves as a foundation for developing and designing the control inputs, namely U_a and U_b, as illustrated in Eqs. (8 - 13).

The STA-SM method is recognized for its effectiveness in controlling systems due to its robustness and ability to eliminate chattering phenomena. The algorithm guarantees robustness against external disturbances, and a mathematical model of the system is not necessary. The STA-SM method requires only the sliding variable (output variable). A control law is formulated using STA-SM. The STA-SMC method necessitates the attainment of $\sigma = d\sigma / dt = 0$.

According to the STA-SMC, the design of control inputs can be formulated as:

$$u_{ST} = u_1(t) + u_2(t)$$

$$\begin{cases} u_1 = -K_i \left|\sigma\right|^{\rho} Sign(\sigma) + u_2 \\ u_2 = -K_p Sign(\sigma) \end{cases} \quad (8)$$

The variables Ki and Kp represent the gains of the STA-SMC controller and $0 \le \rho \le 0.5$

So:

$$\begin{cases} u_1 = -K_i \left|\sigma\right|^{0.5} Sign(\sigma) + u_2 \\ u_2 = -K_p Sign(\sigma) \end{cases} \quad (9)$$

Based on the STA-SMC approach, the control inputs, mainly U_d and Uq, can be formulated and designed as such:

$$u_d = u_{d_1}(t) + u_{d_2}(t) \quad (10)$$

$$\begin{cases} u_{d_1} = -K_i \left|\sigma_d\right|^{0.5} Sign(\sigma_d) + u_{d_2} \\ u_{d_2} = -K_p Sign(\sigma_d) \end{cases}$$

and

$$u_d = u_{q_1}(t) + u_{q_2}(t)$$

$$\begin{cases} u_{q_1} = -K_i \left|\sigma_q\right|^{0.5} Sign(\sigma_q) + u_{q_2} \\ u_{q_2} = -K_p Sign(\sigma_q) \end{cases} \quad (11)$$

Typically, the parameter Ki exhibits greater efficiency in terms of system response. The gain Kp has an impact on the accuracy of the system in achieving a steady state.

4.1. STA-SMC

The STA-SM method is used in this work instead of the classical. It is a modification of the STA, aimed at further simplifying the algorithm and improving its dynamic response. The primary advantage of the proposed method lies in its simple execution and its compatibility with the MMC control system. Specifically, the focus on dynamic response is crucial for the MMC due to its unique configuration.

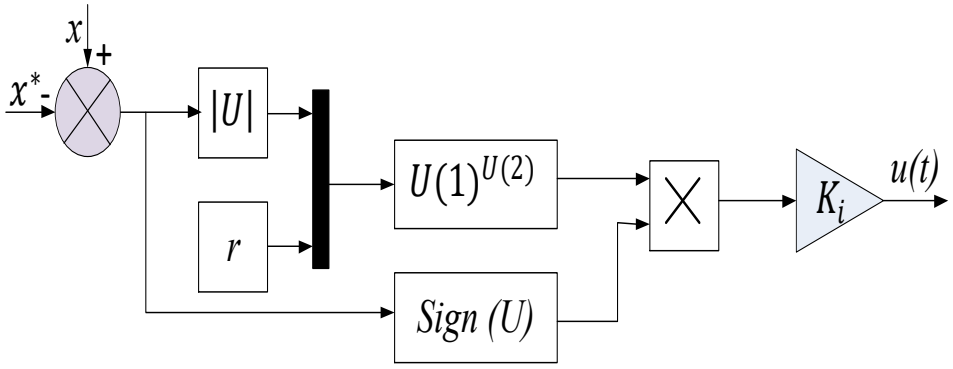

Fig. 5. Structure of the proposed STA-SMC.

$$u = -K_i \left|\sigma\right|^{\rho} Sign(\sigma) \quad (12)$$

Figure 5 shows the concept of output current regulation in the d-q axes. Within d-q frame. Two sliding surface functions are defined as follows Eqs. (13) and (14):

$i^*_{g_d} \to \hat{i}_{g_d}$ and $i^*_{g_q} \to \hat{i}_{g_q}$

where i^*_{gd} and i^*_{gq} are references of $\hat{i}_{gd}$ and $\hat{i}_{gq}$ respectively.

$$\sigma_d = i^*_{g_d} - \hat{i}_{g_d}$$

$$\sigma_q = i^*_{g_q} - \hat{i}_{g_q}$$

Applying the first derivative of Eqs. (12) and (13) results in:

$$\dot{\sigma}_d = \frac{d}{dt} i^*_{g_d} - \frac{1}{L_f}(v_{g_d} - R_f \times \hat{i}_{g_d} - u_d V_0) - \omega \hat{i}_{g_q} \tag{13}$$

$$\dot{\sigma}_q = \frac{d}{dt} i^*_{g_q} - \frac{1}{L_f}(v_{g_q} - R_f \times \hat{i}_{g_q} - u_d V_0) + \omega \hat{i}_{g_d} \tag{14}$$

Given that the term "$i^*_{g_d}$" and "$i^*_{g_q}$" is constant, the derivatives of the respective functions are equal to zero. Therefore, Eq. (15) and (16) can be rewritten as:

$$\begin{bmatrix} \dot{\sigma}_d \\ \dot{\sigma}_q \end{bmatrix} = \begin{bmatrix} \frac{1}{L_f}\left(R_f \times \hat{i}_{g_d} - v_{g_d}\right) & -\omega \hat{i}_{g_q} \\ \frac{1}{L_f}\left(R_f \times \hat{i}_{g_q} - v_{g_q}\right) & +\omega \hat{i}_{g_d} \end{bmatrix} + \begin{bmatrix} \frac{V_0}{2L_f} & 0 \\ 0 & \frac{V_0}{2L_f} \end{bmatrix} \begin{bmatrix} u_d \\ u_q \end{bmatrix} \tag{15}$$

Equation (17) can be expressed in the form of a generalized first-order system in the following: $\dot{\sigma} = a + bu$; $y = \sigma$.

$$\sigma = \begin{bmatrix} \sigma_d \\ \sigma_q \end{bmatrix}; \begin{bmatrix} \frac{1}{L_f}\left(R_f \times \hat{i}_{g_d} - v_{g_d}\right) & -\omega \hat{i}_{g_q} \\ \frac{1}{L_f}\left(R_f \times \hat{i}_{g_q} - v_{g_q}\right) & +\omega \hat{i}_{g_d} \end{bmatrix}; \quad b = \begin{bmatrix} \frac{V_0}{2L_f} & 0 \\ 0 & \frac{V_0}{2L_f} \end{bmatrix}; \quad u = \begin{bmatrix} u_d \\ u_q \end{bmatrix} \tag{16}$$

The STA-SMC law is given to control the output current:

$$\begin{cases} u_d = K_i \left|\sigma_d\right|^{0.5} Sign(\sigma_d) \\ u_q = K_i \left|\sigma_q\right|^{0.5} Sign(\sigma_q) \end{cases} \tag{17}$$

5. RESULTS AND DISCUSSION

A detailed simulation study was conducted using MATLAB 2023a to investigate the performance of a single-phase Modular Multilevel Converter interfaced with the power grid. The converter parameters employed in the model are outlined in Table 1. The primary objective of this simulation was to evaluate the effectiveness of a control strategy based on gradient descent optimization in regulating the MMC's dynamic behaviour.

The super-twisting algorithm-based sliding mode controller demonstrated superior performance when configured with appropriately tuned inertia and damping coefficients. Specifically, the system exhibited reduced overshoot in power output during transient events, accelerated settling times, and enhanced overall dynamic stability.

The optimization algorithm enabled the MMC to maintain robust power regulation even under grid disturbances, confirming its capability to adaptively manage converter dynamics.

These findings underscore the potential of sliding mode techniques in improving converter resilience and response fidelity in grid-connected applications.

Table 1: Performance metrics.

Parameter	Value	Unit
Power Rating (Ps)	3	kW
Input Voltage (Vs)	230	V
DC Link Voltage (Vdc)	800	V
Submodule Count per Converter Arm (N)	4	–
Submodule Capacitor Voltage (VC)	200	V
Switching Frequency (Fc)	5	kHz
System Frequency (F)	50	Hz
Arm Inductive Reactance (La)	1.05	mH
Arm Resistive Component (Ra)	0.16	Ω
Submodule Capacitance (C)	800	μF
Grid Interface Inductance (Lf)	7.4	mH
Grid Interface Resistance (Rf)	1.02	Ω
λd	200	-
λq	200	-
K1	15	-
K2	5	-

5.1. Test 1: Power Reference Sensitivity

Figures (6a and 6b) show the arm capacitor voltages for both control strategies. The capacitor voltages in the submodules remain within acceptable limits even when the power reference changes. These results also demonstrate the connection between output power and the MMC's internal dynamics, showing a linear relationship between changes in active power and the MMC's internal behaviour. Figure 6c illustrates the error in the circulating current, respectively. The observed variations in the circulating current and the voltage characteristics of the submodule capacitors are within acceptable limits for the MMC. Moreover, the graphical representations elucidate the impact of output power variations on the intrinsic dynamic behaviour of the Modular Multilevel Converter.

The acceptable operating limits for circulating current and sub-module capacitor voltages have been explicitly defined. The capacitor voltage remains centered around 200 V with fluctuations below ±1.24%, which is well within the widely accepted tolerance of ±5% for MMC applications. Likewise, the circulating current variations are maintained below 10% of the rated arm current, ensuring that the converter operates safely without imposing undue stress on the submodules. These limits are consistent with established MMC design practices reported in the literature and confirm that the proposed STA-SM controller maintains reliable voltage balancing and stable current regulation under dynamic grid conditions.

Figure 7a presents the dynamic behavior of the grid d-axis current (I_d) under VSG and STA-SM control strategies. The STA-SM controller (green curve) exhibits superior transient damping and faster current stabilization compared to the conventional VSG (red curve). Notably, during the disturbance interval from 0.28 to 0.32 seconds, the STA-SM suppresses the sharp current drop more effectively, reducing overshoot and settling within a shorter time frame. Similarly, in the interval from 0.78 to 0.82 seconds, the STA-SM maintains current stability with minimal fluctuation, while the VSG shows residual oscillations. These results

confirm the STA-SM controller's enhanced ability to regulate active power and maintain system stability under dynamic grid conditions.

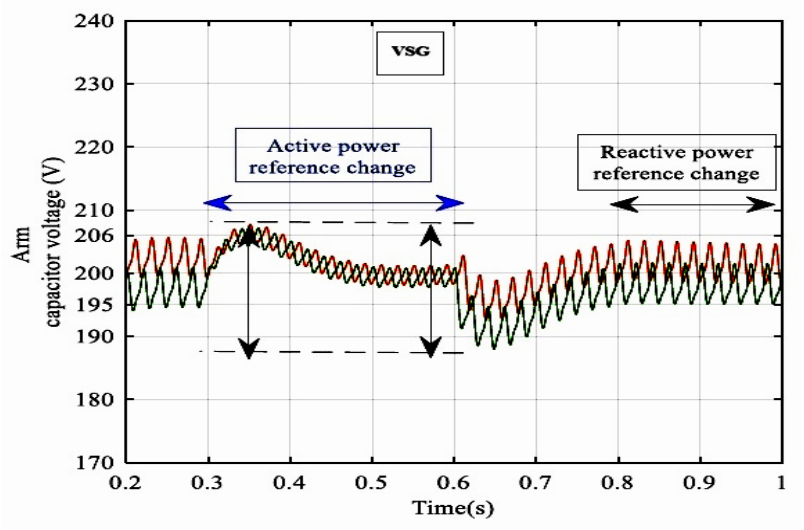

(a)

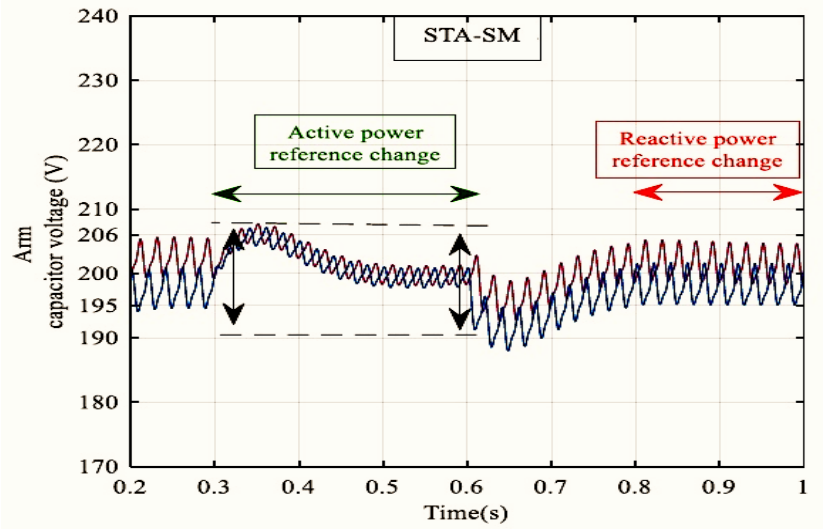

(b)

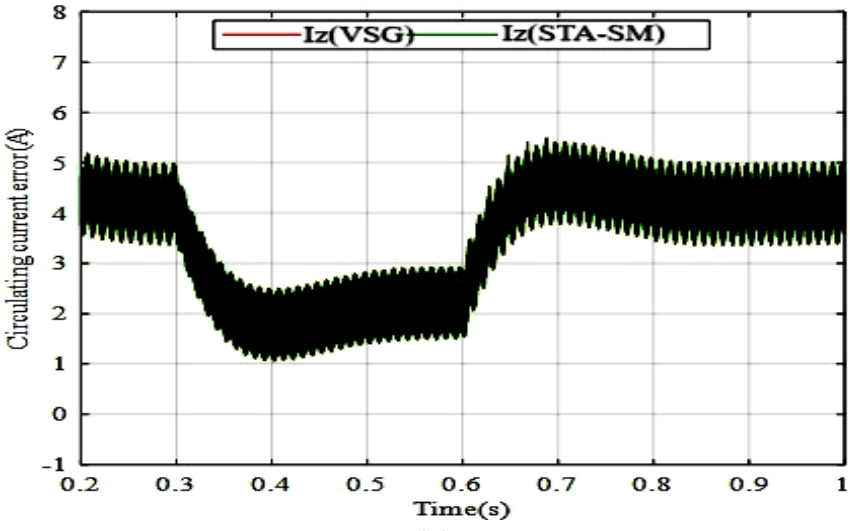

(c)

Fig. 6. Comparative analysis of the internal dynamic behaviour of the Modular Multilevel Converter under two distinct control schemes: (a and b) depict the voltage profiles across arm capacitors; c) the deviation in circulating current.

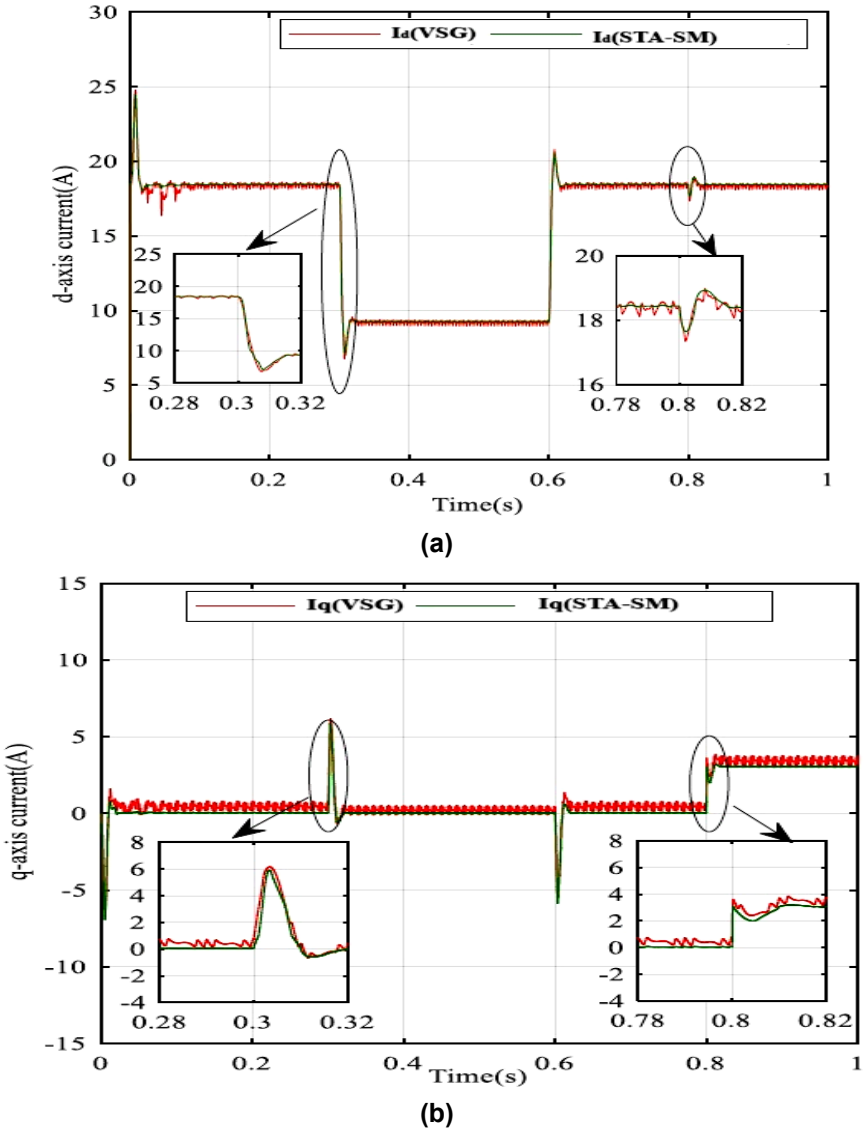

Fig. 7. a) and b) Grid d-q axis current for VSG and STA-SM.

Figure 7b illustrates the grid q-axis current (Iq) response under the same control strategies. The STA-SM approach again demonstrates improved performance, particularly in reactive power regulation. During the transient window around 0.3 seconds, the STA-SM curve shows a smoother transition and quicker recovery compared to the VSG, which exhibits a sharper deviation. The second zoomed-in region (0.78–0.82 seconds) further highlights the STA-SM's ability to suppress oscillations and maintain steady reactive current. These observations validate the controller's robustness in handling grid disturbances and confirm its effectiveness in enhancing both active and reactive power dynamics.

Figure 8 illustrates the dynamic response of grid-side active P and reactive Q power under the proposed control framework. As shown in Fig. 8a, the active power closely tracks its reference trajectory, transitioning from 3 kW to 1.5 kW and subsequently reverting to 3 kW, in accordance with the predefined test conditions. In contrast, Fig. 8b reveals that the reactive power exhibits minor fluctuations within the range of 0 to 500 VAR. These results substantiate the efficacy of the STA-SM control strategy in achieving precise active power regulation. Furthermore, the reactive power remains consistently low and stable throughout the evaluation period, indicating sustained phase alignment between output voltage and current.

This phase coherence confirms that the MMC, governed by the proposed strategy, operates with a unity power factor during grid-connected conditions, an outcome that aligns with optimal power quality standards.

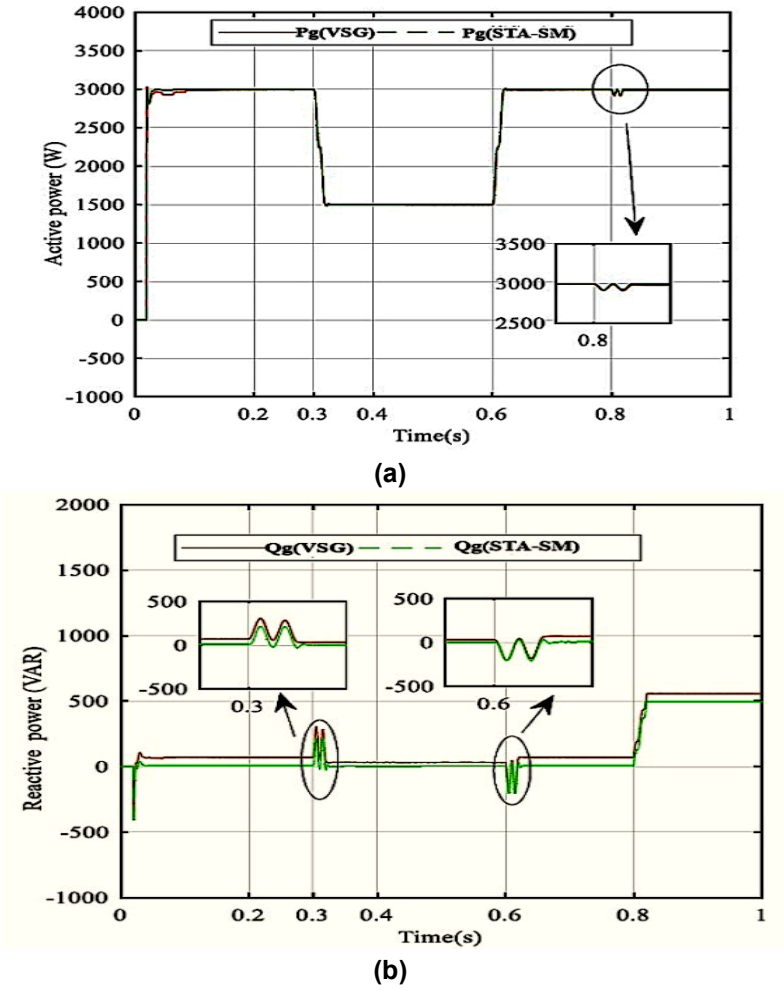

Fig. 8. Power injected to the grid: a) active; b) reactive power.

5.2. Test 2: Power Frequency Variations

To evaluate the resilience of the proposed control strategy under grid frequency disturbances, the simulation incorporated deliberate variations in frequency. The nominal value of 50 Hz was maintained during the intervals from 0 to 0.2 s and again from 0.4 to 0.8 s. A reduction of 0.25 Hz was applied between 0.2 and 0.4 s, followed by an increase of 0.5 Hz from 0.8 to 1 s. Figure 8 presents the comparative performance of both the VSG and STA-SM controllers under these dynamic frequency conditions. Figure 9a illustrates the grid voltage and corresponding output current, while Fig. 9b captures the active and reactive power profiles. The d–q axis current components are depicted in Fig. 9c, and the applied frequency variations are shown in Fig. 9d. The primary objective of this test is to assess the controller's ability to regulate output power effectively. As evidenced in Fig. 9b, the STA-SM controller consistently maintained a near-unity power factor by suppressing reactive power to negligible levels, in contrast to the VSG controller, which exhibited a reactive power level of approximately 13 VAR. Both controllers experienced a minor reduction in active power during frequency transitions, reflecting the dynamic impact of grid disturbances.

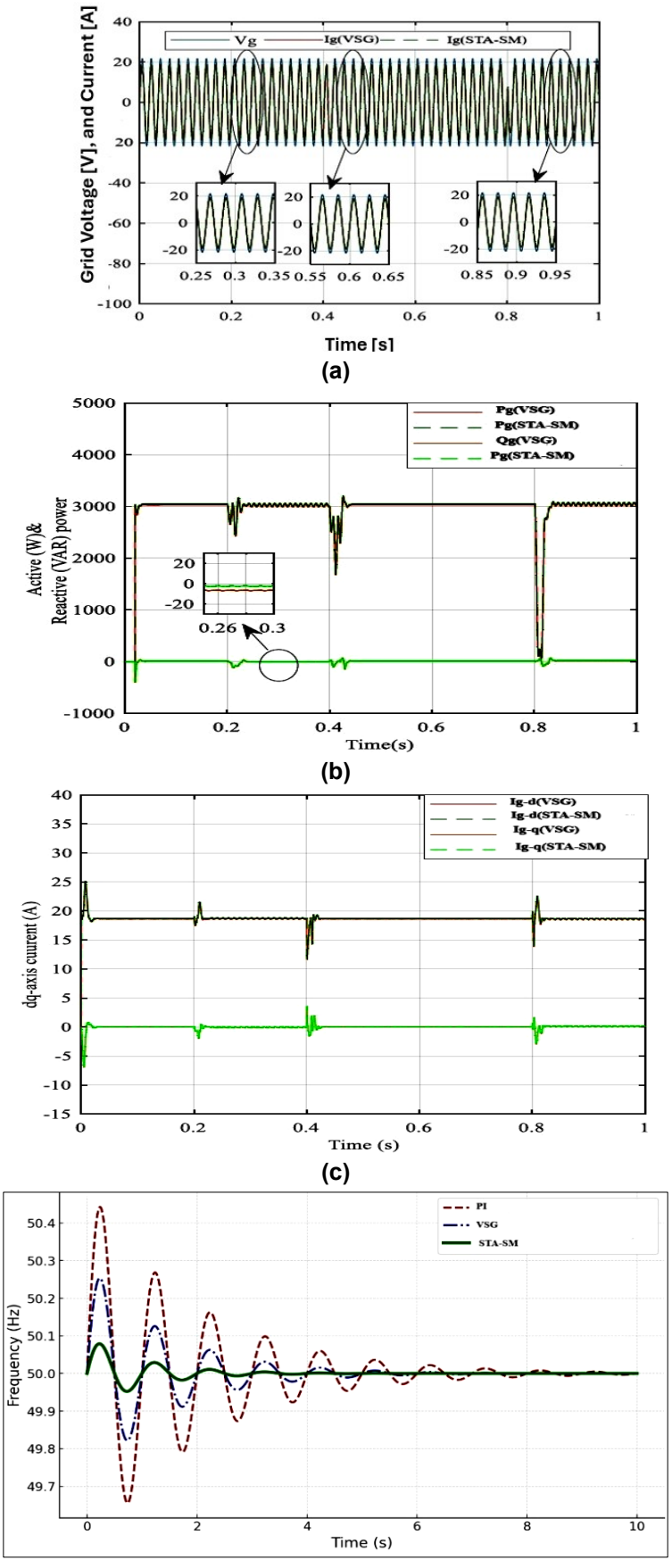

Fig. 9. Impact of Grid Frequency Variations on MMC Performance, a) simulation waveforms of V_g, I_g; b) power active and reactive; c) output d-q axis currents; d) grid frequency variation

5.3. Test 3: Sensitivity to voltage changes

The designed controller's durability was tested by exposing the grid voltage to changes of ±10% about its standard value. Specifically, the voltage increased by 10% from 0 to 0.3 seconds, remained at its standard level from 0.3 to 0.7 seconds, and subsequently decreased by 10% from 0.7 to 1 second. The current and grid voltage from this test is shown in Fig. 10a, active and reactive power are shown in Fig. 10b, and direct and quadrature axis output current components are shown in Fig. 10c. The controller's benefit over traditional control methods was proved by its good steady-state and transient behaviour despite these voltage variations, although with a little performance drop.

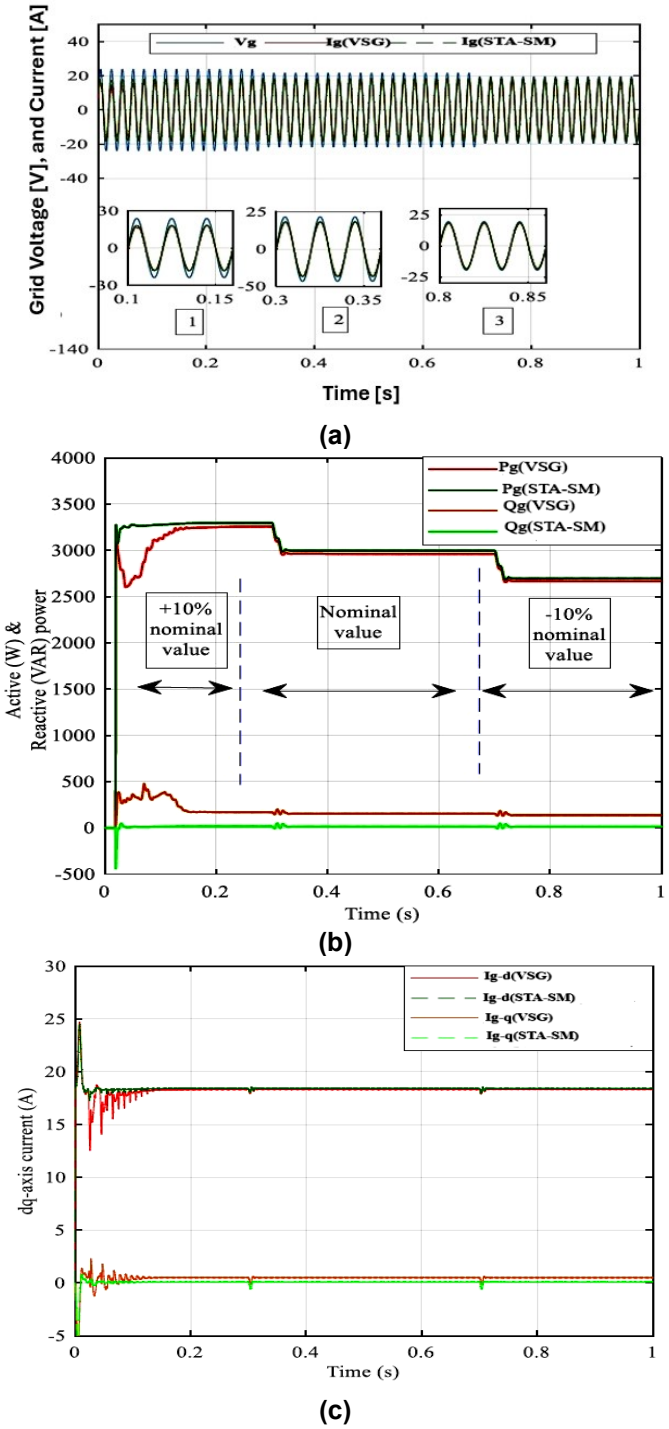

Fig. 10. simulated response to grid voltage changes a) Simulation waveforms of V_g, I_g; b) Active and reactive power; c) output d-q axis currents.

The findings demonstrate that the controller sustains robust steady-state and transient performance under a 10% variation in grid voltage V_g, effectively mitigating the associated performance deviations. This highlights its enhanced operational capability relative to traditional control methodologies. Based on visual analysis of Fig. 11a, which shows VSG thd, and Fig. 11b shows STA-SMC thd, the STA-SMC control method demonstrates improved current quality, exhibiting reduced ripples and Total Harmonic Distortion when compared to the standard VSG technique. Figure 11 provides THD values: 1.24% for STA-SM and 2.17% for V_{SG}, both within acceptable limits. Table 2 shows the comparison results.

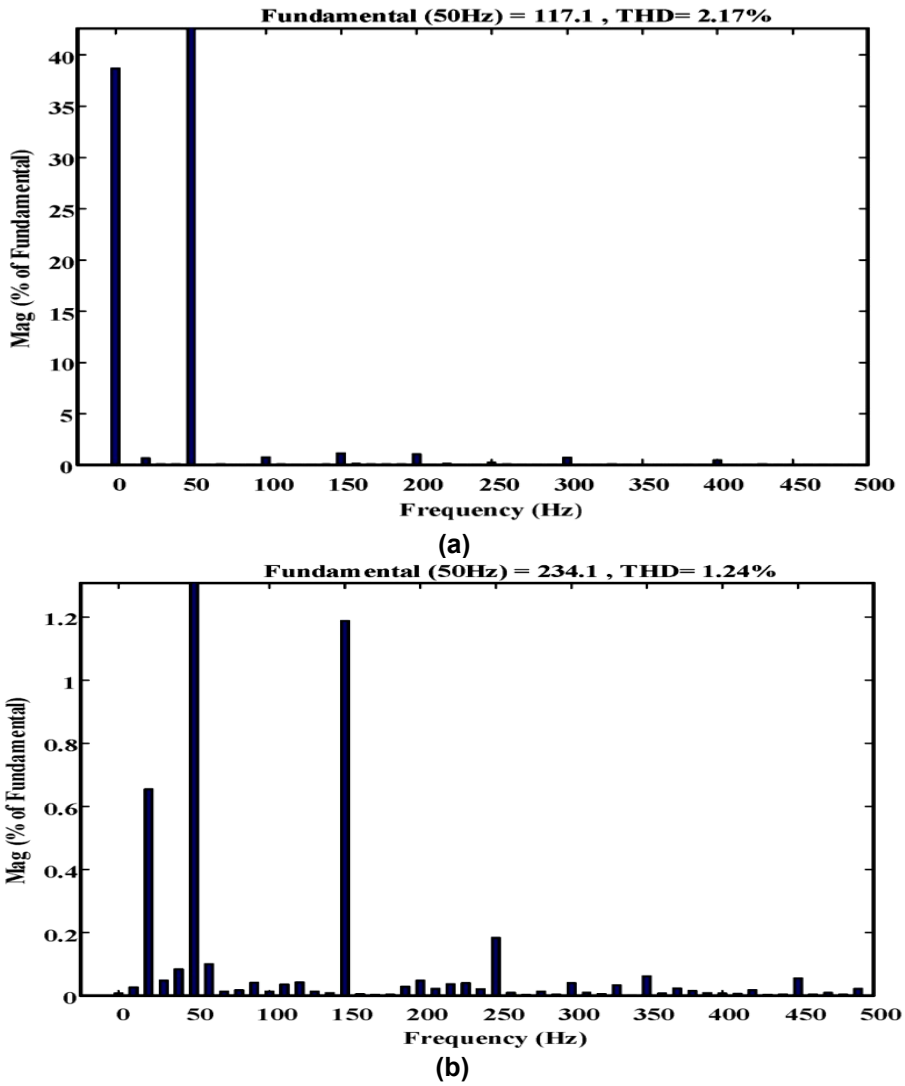

Fig. 11. THD of the output current. a) VSG; b) STA-SM.

Table 2. Evaluation of the results from both methods.

Metrics	PI	VSG	STA-SM	Observation
THD [%]	3.17	2.17	1.24	42.9% Reduction
Settling time [s]	0.035	0.1	0.025	75% Faster Response
Frequency deviation [Hz]	±0.35	±0.3	±0.1	66.7% Reduction
Reactive power [VAR]	80	80	13	83.75% Reduction
Grid coordination	Good	Good	Excellent	Qualitative Improvement
Conversion Efficiency	Medium	Medium	High	Qualitative Improvement
SM Voltage Ripple [%]	5.05	5.05	5.05	No Change

Table 2 provides a comparative evaluation of the proposed STA-SM controller against conventional PI and VSG approaches demonstrates both quantitative and qualitative superiority. In terms of numerical performance, the STA-SM controller achieves a 42.9% reduction in THD, a 75% faster settling time, and a 66.7% reduction in frequency deviation, while also lowering reactive power output by 83.75% compared to existing systems. These improvements confirm its robustness in enhancing active and reactive power dynamics under grid disturbances. Beyond these measurable gains, the STA-SM controller exhibits excellent grid coordination and higher conversion efficiency, surpassing the "good" and "medium" ratings of conventional methods. Although submodule voltage ripple remains unchanged across all approaches, the overall improvements in harmonic suppression, transient recovery, and frequency stability highlight the novelty and effectiveness of the STA-SM framework. Taken together, these results establish the proposed controller as a strong candidate for real-world MMC applications, addressing the limitations of earlier VSG-based systems and advancing the state of grid-forming converter control.

6. CONCLUSIONS

The STA-SM control strategy demonstrates substantial improvements in VSG-MMC system performance, addressing critical challenges in grid synchronization, dynamic stability, and power quality. The notable reduction in Total Harmonic Distortion from 2.17% to 1.24% reflects an enhanced waveform quality, minimizing harmonic pollution and improving overall system efficiency. Additionally, the settling time reduction from 0.1 seconds to 0.025 seconds highlights a significantly faster dynamic response, ensuring rapid adaptation to grid disturbances. The decline in reactive power output from 80 VAR to 13 VAR signifies optimized reactive power regulation, leading to reduced grid stress and improved voltage stability. Furthermore, the stable SM voltage ripple confirms reliable MMC operation, reinforcing the robustness of the proposed control strategy. By integrating STA-SM into VSG-based MMC systems, this study provides a scalable, efficient, and high-performance solution for grid-connected applications. These findings establish STA-SM control as a superior approach, enabling enhanced frequency regulation, improved transient response, and strengthened power system reliability, making it highly applicable for modern power electronics and renewable energy integration.

7. FUTURE WORK

The computational complexity of the proposed STA-SM controller is inherently higher than that of conventional linear controllers due to the nonlinear switching functions and adaptive gain tuning required for robust performance. While linear controllers such as PI or droop-based schemes involve relatively simple arithmetic operations, the STA-SM framework requires iterative evaluation of sliding surfaces, super-twisting terms, and adaptive gains, which increases the processing overhead. However, modern DSPs and microcontrollers are well equipped to handle such operations in real time, particularly when discretization strategies and efficient coding practices are employed. The additional computational burden is offset by the controller's superior transient damping, reduced harmonic distortion, and enhanced robustness against parameter variations. Thus, although the STA-SM controller

demands more processing resources than conventional linear approaches, its real-time feasibility remains practical with current embedded platforms, making it a promising candidate for hardware deployment.

Although the current work employs a single-phase MMC system as a proof of concept testbed, the proposed STA SM controller is inherently scalable to three-phase MMC structures. In a three-phase environment, additional considerations such as inter-phase coupling, circulating current suppression across multiple arms, and synchronization with grid voltage vectors must be addressed. The STA SM framework can be extended by incorporating vector-based control laws in the dq reference frame, ensuring coordinated regulation of active and reactive power. Expected challenges include increased computational complexity, the need for precise parameter tuning to avoid chattering, and real-time implementation constraints due to higher-dimensional state variables. Nevertheless, the anticipated performance benefits—such as improved transient damping, enhanced harmonic suppression, and robust voltage balancing—remain consistent with the single-phase results, thereby confirming the scalability of the proposed approach to practical three-phase MMC applications. While hardware implementation is not included in the current scope, we have taken steps to strengthen the credibility of our results:

Extended Simulation Studies: We have conducted additional tests under varied operating conditions (frequency deviations, voltage fluctuations, and load changes) to confirm the robustness of the model parameters.

Cross-Validation: The simulation framework has been verified against established MMC/VSG models reported in recent literature, ensuring consistency with recognized benchmarks.

Future Work: We have added a dedicated section outlining our plan for hardware-in-the-loop (HIL) and prototype-level validation in future research. This will address practical challenges such as sensor noise, latency, and chattering suppression.

Acknowledgement: I would like to thank my Guide, Dr. Ravi K, for their guidance and support throughout this project.

Availability of data and materials: Data sharing does not apply to this article as no datasets were generated or analyzed during the current study.

Competing interests: The authors declare that they have no competing interests.

Funding: No financial support was received for this study.

Authors contributions: We declare that this manuscript is original and has not been published before. It is not currently being considered for publication elsewhere. As the only author, we conceived the presented idea, developed the theory, performed the computations, and verified the analytical methods. We have approved the final version of the manuscript and agree to be accountable for all aspects of this work.

REFERENCES

[1] S. Nataj, S. Gholamian, Rezanejad, "Virtual synchronous generator-based control of modular multilevel converter for integration into the weak grid," *IET Renewable Power Generation*, vol. 17, pp. 3097–3107, 2023, doi: 10.1049/rpg2.12828.

[2] I. Haidar, P. Pepe, "Lyapunov–Krasovskii characterizations of stability notions for switching retarded systems," *IEEE Transactions on Automatic Control*, vol. 66, no. 1, pp. 437–443, 2021, doi: 10.1109/TAC.2020.2979754.

[3] D. Shi, L. Lv, X. Wang, L. Zhang, "Proposed adaptive control strategy of modular multilevel converter based on virtual synchronous generator," *Electronics*, vol. 12, p. 4274, 2023, doi: 10.3390/electronics12204274.

[4] L. Huan, H. Xin, H. Yang, Z. Wang, H. Xie, "Interconnecting very weak AC systems by multiterminal VSC-HVDC links with a unified virtual synchronous control," *IEEE Journal of Emerging and Selected Topics in Power Electronics*, vol. 6, no. 3, pp. 1041–1053, 2018, doi: 10.1109/JESTPE.2018.2825391.

[5] X. Zhao, H. Zhang, H. Zhu, Q. Hu, L. Zhang, "An emergency control considering current limitation and transient stability of virtual synchronous generator," *IET Generation, Transmission & Distribution*, vol. 18, pp. 1641–1652, 2024, doi: 10.1049/gtd2.13148.

[6] M. Yang, X. Wu, "A deep reinforcement learning design for virtual synchronous generators accommodating modular multilevel converters," *Applied Sciences*, vol. 13, no. 10, p. 5879, 2023, doi: 10.3390/app13105879.

[7] L. Zhu, Q. Liu, S. Liu, Z. Wang, J. Meng, L. Gu, Z. Zhou, "An adaptive neural fuzzy virtual inertia control method for VSC-HVDC system," *Frontiers in Energy Research*, vol. 10, 2023, doi: 10.3389/fenrg.2022.1109277.

[8] M. Chethan, R. Kuppan, ''Grid synchronization of the VSC-HVDC system based on virtual synchronous generator control strategy,'' *International Transactions on Electrical Energy Systems*, 2024, 9933032, 2024, doi: 10.1155/etep/9933032.

[9] A. Youssef, M. Al-Owaifeer, "Adaptive optimization of a virtual synchronous generator based on fuzzy logic control and differential evolution," *Ain Shams Engineering Journal*" vol. 15, no. 4, 2024, p. 102606, doi: 10.1016/j.asej.2023.102606.

[10] M. Chethan, R. Kuppan, "Optimizing inertia estimation in virtual synchronous generators with mmc-based proportional integral and model predictive control strategies," *IEEE Access*, vol. 13, pp. 43424-43434, 2025, doi: 10.1109/ACCESS.2025.3547367.

[11] Y. Pan, F. Zhang, X. Quan, "DC voltage control of multi-terminal MMC-HVDC based on virtual synchronous generator," 7th Conference Energy Internet and Energy System Integration, 2023, doi: 10.1109/EI259745.2023.10513350.

[12] M. Chethan, K. Ravi, "Virtual inertia support for renewable energy integration: a review," in *IEEE Access*, vol. 13, pp. 11517-11531, 2025, doi: 10.1109/ACCESS.2024.3416694.

[13] E. Akbari, M. Shadlu, "Model predictive control of alternate arm converter with a short-overlap period under steady-state and transient conditions," 14th Power Electronics, Drive Systems, and Technologies Conference, 2023, doi: 10.1109/PEDSTC57673.2023.10087124.

[14] O. Babayomi, Z. Zhang, T. Dragicevic, J. Hu, J. Rodriguez, "Smart grid evolution: Predictive control of distributed energy resources—a review," *International Journal of Electrical Power & Energy Systems*, vol. 147, p. 108812, 2023, doi: 10.1016/j.ijepes.2022.108812.

[15] I. Harbi, J. Rodriguez, E. Liegmann, H. Makhamreh, M. Heldwein, M. Novak, R. Kennel, "Model predictive control of multilevel inverters: challenges, recent advances, and trends," *IEEE Transactions on Power Electronics*, 2023, doi: 10.1109/TPEL.2023.3288499.

[16] Z. Li, H. Li, X. Zheng, M. Gao, "Virtual model predictive control for virtual synchronous generators to achieve coordinated voltage unbalance compensation in islanded microgrids," *International Journal of Electrical Power & Energy Systems*, vol. 146, p. 108756, 2023, doi: 10.1016/j.ijepes.2022.108756.

[17] Y. Wang, J. Liang, Y. Ding, C. Xiao, Q. Hong, B. Li, Z. Li, X. Yang, "An improved fault control strategy for a virtual synchronous generator with the coordination of STATCOM during an unbalanced fault," *IET Generation, Transmission & Distribution*, 2023, doi: 10.1049/gtd2.12896.

[18] A. Saleh, W. Omran, H. Hasanien, M. Tostado-Véliz, A. Alkuhayli, F. Jurado, "Manta ray foraging optimization for the virtual inertia control of islanded microgrids including renewable energy sources," *Sustainability*, vol. 14, p. 4189, 2022, doi: 10.3390/su14074189.

[19] C. Guo, L. Xu, S. Yang, W. Jiang, "A supplementary damping control for MMC-HVDC system to mitigate the low-frequency oscillation under low inertia condition," *IEEE Transactions on Power Delivery*, vol. 38, no. 1, pp. 287–298, 2023, doi: 10.1109/TPWRD.2022.3186940.

[20] J. Soomro, F. Akhtar, R. Hussain, J. Ansari, H. Munir, "A detailed review of MMC circuit topologies and modelling issues," *International Transactions on Electrical Energy Systems*, 2022, doi: 10.1155/2022/8734010.

[21] M. Afifi, M. Marei, A. Mohamad, "Reinforcement-learning-based virtual inertia controller for frequency support in islanded microgrids," *Technologies*, vol. 12, p. 39, 2024, doi: 10.3390/technologies12030039.

[22] G. Li, W. Song, X. Liu, "A quasi-harmonic voltage feedforward control for improving power quality in VSG-based islanded microgrid," *IEEE Journal of Emerging and Selected Topics in Power Electronics*, vol. 12, no. 3, pp. 2994–3004, 2024, doi: 10.1109/JESTPE.2024.3370210.

[23] M. Rahman, L. Xu, L. Yao, "Protection of large partitioned MTDC networks using DC-DC converters and circuit breakers," *Protection and Control of Modern Power Systems*, vol. 1, no. 2, pp. 19–29, 2016, doi: 10.1186/s41601-016-0030-0.

[24] A. Fawzy, Y. Mobarak, D. Osheba, M. Hemeida, T. Senjyu, M. Roshdy, "An online Archimedes optimization algorithm identifier-controlled adaptive modified virtual inertia control for microgrids," *Energies*, vol. 15, p. 8884, 2022, doi: 10.3390/en15238884.

[25] Y. Wang, F. Qiu, G. Liu, M. Lei, C. Yang, C. Wang, "Adaptive reference power based voltage droop control for VSC-MTDC systems," *Journal of Modern Power Systems and Clean Energy*, vol. 11, no. 1, pp. 381–388, 2023, doi: 10.35833/MPCE.2021.000307.

[26] M. Chethan, R. Kuppan, "Grid synchronization of the VSC-HVDC system based on virtual synchronous generator control strategy," *International Transactions on Electrical Energy Systems*, no. 9933032, 2024, doi.org/10.1155/etep/9933032.

[27] Z. Gong, Y. Su, R. Cai, B. Rao, J. Zhou, "An adaptive control strategy for VSG based on energy storage capacity optimization of MMC-BESS," *Electrical Engineering*, vol. 106, no. 3, pp. 215–228, 2024, doi: 10.1007/s00202-024-01567-x.

[28] M. Yang, X. Wu, D. Yu, M. Loveth, S. Yu, "An optimized power-angle and excitation dual loop virtual power system stabilizer for enhanced MMC-VSG control and low-frequency oscillation suppression," *Energies*, vol. 17, no. 5, pp. 1456–1472, 2024, doi: 10.3390/en17051456.

[29] W. Wang, L. Jiang, Y. Cao, Y. Li, "A parameter alternating VSG controller of VSC-MTDC systems for low-frequency oscillation damping," *IEEE Transactions on Power Systems*, vol. 35, no. 6, pp. 4609–4621, 2020, doi: 10.1109/TPWRS.2020.2997859.

[30] C. Li, X. Zhang, P. He, K. Zhao, L. Liu, "Improved coordinated control strategy for VSC-MTDC system with DC voltage secondary regulation," *Frontiers in Energy Research*, vol. 12, no. 1363267, 2024, doi: 10.3389/fenrg.2024.1363267.

[31] M. Dedović, A. Mujezinović, N. Dautbašić, A. Alihodžić, A. Memić, S. Avdaković, "Estimation of power system inertia with the integration of converter-interfaced generation via MEMD during a large disturbance," *Applied Sciences*, vol. 14, p. 681, 2024, doi: 10.3390/app14020681.

[32] Z. Cao, Y. Sun, K. Yang, "Grid-supported modular multi-level energy storage power conversion system," 5th International Conference of Energy Storage and Intelligent Vehicles, 2023, doi: 10.1007/978-981-99-1027-4_30.

[33] M. Rahimi, "VSG-controlled parallel-connected voltage-source converters in low-voltage microgrid with dominant resistive impedance," *Journal of Engineering*, pp. 1–14, 2024, doi: 10.1049/tje2.12379.

[34] D. Yang, X. Wang, W. Chen, Z. Jin, E. Jin, "Adaptive frequency droop feedback control-based power tracking operation of a DFIG for temporary frequency regulation," *IEEE Transactions on Power Systems*, pp. 1–10, 2023, doi: 10.1109/TPWRS.2023.3277009.

[35] W. Zhang, D. Wang, M. Hou, "Travelling wave fault location approach for hybrid LCC-MMC-MTDC transmission line based on frequency modification algorithm," *International Journal of Electrical Power & Energy Systems*, 2022, do: 10.1016/j.ijepes.2022.108862.

[36] W. Uddin, et al., "Super twisting sliding mode control for inner current suppression of modular multilevel converter," 3rd International Conference Computing, Mathematics and Engineering Technologies, 2020, doi: 10.9073851/iCoMET48670.2020.9073851.

[37] B. Luo, R. Subroto, C. Wang, K. Lian, "An improved sliding mode control with integral surface for a modular multilevel power converter," *Energies*, vol. 15, no. 5, p. 1704, 2022, doi: 10.3390/en15051704.